

CARBON ARC DISCHARGE: PLASMA EMISSION SPECTROSCOPY AND CARBON NANOSTRUCTURE FORMATION

H. Lange, A. Huczko

Department of Chemistry, Warsaw University, Warsaw, Poland
Fax: +48 22 8225996, e-mail: lanhub@chem.uw.edu.pl

Emission spectroscopy with the self-absorption consideration in ($d^3\Pi_g - a^3\Pi_u, 0-0$) Swan band was performed to determine C_2 radical content and temperature in the carbon arc plasmas generated in helium and water between pure and catalyst-doped graphite electrodes. Morphology of produced nanocarbons was investigated by scanning and transmission electron microscopy.

Key words: carbon plasma, emission spectroscopy, fullerenes, carbon nanotube

1. INTRODUCTION

The arc plasma technique has been known to produce nanopowders and composite nanomaterials for years. The carbon arc found its application in metallurgy a long time ago, while more recently arc-plasma-produced carbon vapors have been shown to be the source of fascinating novel nanocarbons – fullerenes [1,2] and carbon nanotubes (CNTs) [3]. Since the discovery of these new allotropes of carbon an explosion of research has occurred with the application of the arc to their production. A commercial way for fullerene synthesis, developed in 1990 by Krätschmer et al. [2], is based on the arc discharge between graphite electrodes in a helium atmosphere at pressure ca. 13 kPa. Ebbesen and Ajayan [4] first prepared large quantities of CNTs using carbon arc discharge in helium at higher pressures, ca. 60 kPa. It has also been shown that the carbon arc co-evaporation of various elements or compounds may lead to other interesting carbon nanomaterials, e.g., functionalized fullerenes like heterofullerenes and endohedrals [5], filled nanotubes [6], onions [7] and nanoencapsulates [8]. For the synthesis of nanocarbons the arc discharge ignited in helium was considered to be the most suitable medium. However, quite recently the oriented single-walled carbon nanotubes (SWCNTs) were obtained with a very high yield applying arc discharge in a mixture of Ar and H_2 [9]. A carbon arc discharge in liquids also seems to be very promising, particularly in de-ionized water [10] or in a water salt solution [11]. It appeared to be a source of different nanocarbons e.g., nanooxions [10], CNTs filled with a catalyst [11-13], carbon nanohorns and metal-including nanocapsules. Interesting method of continuous production of CNTs in liquid nitrogen has also been elaborated [14]. Many excellent papers have been published so far regarding the application of the arc plasma for nanocarbons production covering many practical aspects. Therefore in this short review only few of them, mostly some recent papers, are reported. Nevertheless, one can conclude that detailed studies of carbon arc discharge are of great interest. Moreover, up to now, partly because of commercial reasons, the majority of studies are focused mostly on a search for the most efficient ways for nanocarbons production. However, recently the gradual increase of interest to

study the mechanism and kinetics of nanocarbons formation in the arc discharge emerged [15].

This work is devoted to plasma characterization through the determination of temperature, plasma composition and yield of fullerenes. The results related to the production of various carbon nanostructures under different arc discharge conditions are also presented.

2. EXPERIMENTAL

2.1. Experimental Set-up

The scheme of the arc discharge system (horizontal cross-section of reactor chamber with movable electrodes) and optical arrangement for spectroscopic measurements is shown in Fig. 1.

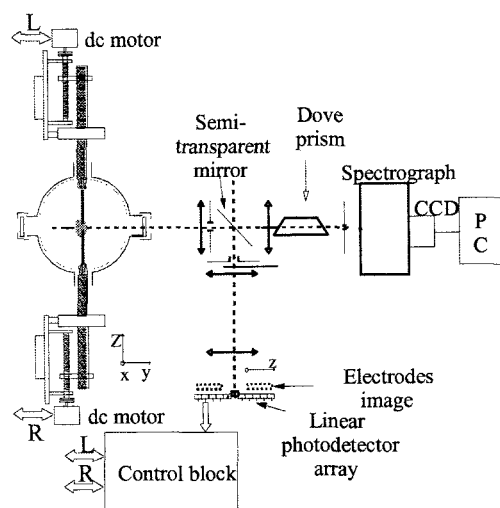


Fig. 1 Experimental set-up.

The system, fully automated, allows digital control of pressure in the reactor chamber, discharge current, anode sublimation rate, electrode gap and its position on the optical axis. The details of the system and procedure is described elsewhere [16]. The arc plasmas were generated in He and in water. Pure and catalyst-doped graphite electrodes (homogeneous or drilled and filled with a catalyst) of 6 mm in diameter were sublimated under different arc discharge conditions.

The products were analyzed using high resolution scanning and transmission electron microscopy (HR SEM and HR TEM).

2.2. Plasma Spectroscopy

It follows from the thermodynamic equilibrium considerations between carbon particles ($C_{n=1-5}$) in the gas phase that at temperatures above 4000 K, which are typical for the carbon arc plasma zone, the major gas components are the carbon atoms, ions and diatomic molecules. Indeed, only emission of these species is observed in the case of pure carbon arc plasma. For plasma diagnostics the most suitable is the Swan band system ($d^3\Pi_g - a^3\Pi_u$), particularly the mostly exploited 0-0 band at 516.5 nm. Since the carbon vapor pressure in the arc under conditions favoring formation of nanocarbons, e.g., fullerenes and CNTs, can be quite high, this band, and mainly its head, is disturbed by the self-absorption phenomenon. Thus we took advantage of this effect for temperature and column density of C_2 radical determination [17]. The column density is defined as the product of the radical concentration (N) and length (L) of plasma column along a line of sight. To our knowledge, excluding a method based on absolute intensity measurement of the Swan band [18], no other reliable quantitative methods for carbon arc plasma characterization have been elaborated so far. Strong light emitted by the carbon arc, high fluctuation of the process of anode ablation, relatively small arc gap (ca. 1 mm) necessary for carbon nanostructure formation, make other methods, e.g. standard absorption or very sensitive laser-induced fluorescence, of a very limited use. The presence of carbon micro-crystallites in the gas phase scattering the radiation along the observation path is also a barrier to precisely measure the light emitted by or passing through the arc. For instant according to our measurements at low-pressure arc discharge (13 kPa) and moderate anode erosion rate (4 mg s^{-1}) the transmittance was about 30 %, while at atmospheric pressure was only 10 %. The transient methods are also not applicable for such a dusty system because decay of C_2 radical is a few orders faster than the process of carbon dust condensation. The latter one takes even seconds while C_2 radicals disappear in microseconds. Hence, the optical emission spectroscopy (OES) associated with the self-absorption consideration seems to be the most suitable method. In this method the experimental spectra, $C_2(d - a, 0-0)$ band, normalized to the band head, are fitted to the computed spectra for various C_2 column densities and temperatures. Such a direct fitting can instantly provide temperature and column density. Temperature can also be evaluated from the Boltzmann plots using resolved rotational components, which obviously are much less self-absorbed than the band head [17]. One has to point out, however, that the applied approach by no means can give local values; it simply leads only to the value somehow close to the average one within a plasma column. It is so also due to the self-absorption phenomenon that any procedure of Abel inversion can not be applied.

3. RESULTS AND DISCUSSION

3.1. Carbon Arc Plasma Characterization

3.1.1. Ar discharge in He

The attention was mainly focused on the influence of the anode (pure graphite) erosion rate and He pressure on the plasma temperature and C_2 content in the arc zone. When erosion rate was controlled by the arc current (between 50 and 95 A) the He pressure was kept constant, 13.3 kPa, and vice versa under different He pressure the erosion rate was adjusted to ca. 4 mg s^{-1} .

The influence of the anode erosion rate on plasma parameters is illustrated in Fig. 2.

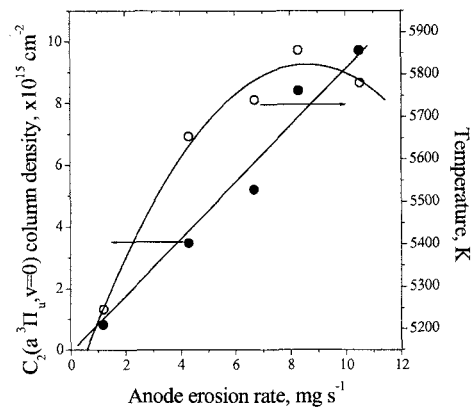


Fig. 2. Temperature and $C_2(a^3\Pi_u, v=0)$ column density vs. anode erosion rate. Pressure: 13.3 kPa. Anode: pure graphite.

The column density can be converted into average density dividing the first one by the optical path which is ca. 1 cm. Subsequently, C_2 density can be used for the estimation of the total carbon pressure assuming the thermodynamic equilibrium.

Evidently a linear dependence takes place between the as determined C_2 column density and anode erosion rate. It follows from Fig. 2 that mean gas temperature in the arc zone is between 5000 and 6000 K and increases with the discharge current.

The influence of He pressure on C_2 content under constant erosion rate is shown in Fig. 3.

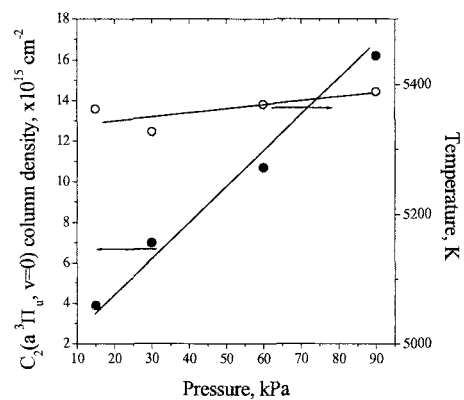


Fig. 3. Temperature and $C_2(a^3\Pi_u, v=0)$ column density vs. pressure. Erosion rate: 3.6 mg s^{-1} . Anode: pure graphite.

With the pressure increase the diffusion of carbon species out of plasma zone is hampered by helium. Hence the observed increase in local C_2 density.

The uncertainty, which follows from the applied approach in C_2 determination has already been investigated [19]. Mostly it gives value higher of the real one. The discrepancy increases with the C_2 column density. So, the linear dependence observed in Figs 2 and 3 can be in fact slightly different.

3.1.3. Arc discharge in water

The experiments were carried out at discharge current equal to 40 A. Pure graphite, as well as homogeneous Gd- or Y-doped electrodes, were employed. It is noteworthy that the discharge in water was erratic, thus it was critical to control precisely the arc gap on the optical axis and to run the discharge smoothly. Therefore the measurements were performed only along the electrodes. The results are shown in Fig. 4.

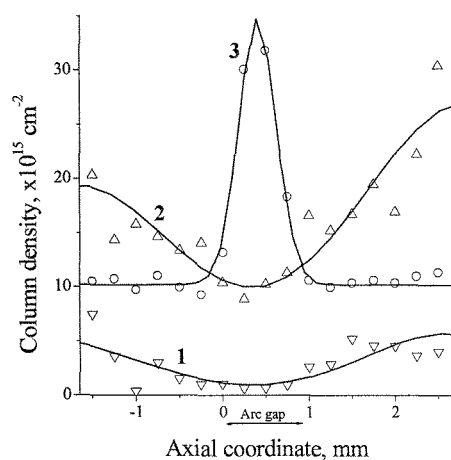


Fig.4. Column density of $C_2(a^3\Pi_u, v=0)$ radical in arc discharge in water. Anode: 1 – C; 2- C + 0.8at% Gd; 3 – C + 0.8 at% Y.

The arc gap position in Fig. 4 is between the coordinates 0 and 1. The erosion rate of pure graphite anode was about 2.5 mg s^{-1} while in the case of Gd- and Y-doped electrodes was ca. 3 and 4 times higher, respectively. Hence, a significant diversity in the axial C_2 column density distributions was observed. Generally, the amount of C_2 produced in water discharge, despite a low current, is higher than that formed in the presence of He, as results from comparison with a test performed under the same discharge current (40 A) and atmospheric pressure. The determined average plasma temperature in water was also quite high, ca. 4000 - 6500 K. It is apparent that the high temperature, despite of low current, results from bubbles, which are small in number and volume, leading to high energy density. Also, the reaction between carbon, oxygen and hydrogen are highly exothermic. Since the plasma is surrounded by water, diffusion is limited within the bubble volume and carbon species are trapped within the bubbles.

3.2. Carbon Nanostructure Synthesis

Graphite electrodes subjected to high current arc discharge undergo sublimation. Carbon vapor partly condenses on the surrounding arc discharge wall as amorphous soot, and partly is transported toward the cathode tip forming the cathode deposit. The cathode deposit and soot may contain carbon nanotubes (CNT), whereas fullerenes are present only in the condensed soot.

3.2.1. Yield of Fullerene C_{60}

The best condition for fullerene synthesis is at pressure ca. 13 kPa. The average content of C_{60} fullerene in the soot resulting from arcing of pure graphite electrodes in function of input power at constant He pressure (13.3 kPa) is shown in Fig. 5.

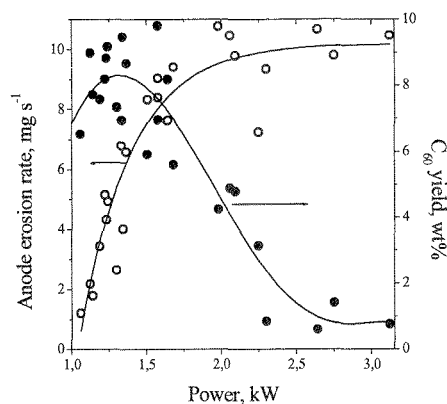


Fig. 5. Anode erosion rate and yield of fullerene C_{60} vs. input power.

The experimental points are scattered; however, this phenomenon – resulting from the high system sensibility towards the change of process parameters – has been always observed for the unstable carbon arc.

The main conclusion of the performed tests is that the best conditions for syntheses of fullerenes are at moderate input power, between 1.2 and 1.5 kW. Then the anode erosion rate is between 4 and 6 mg s^{-1} .

When catalysts are co-evaporated with graphite, the yield of C_{60} usually is reduced, e.g., about twice in the case of Fe, or Co/Ni [20]. In the case of Gd (or Y) – doped electrodes the yield drastically decreases to about 0.4 wt% [21]. This phenomenon is mainly due to the disturbance of carbon atom coalescence by the ‘guest’ atoms.

3.2.2 CNTs and Other Carbon Nanostructures

A cathode deposit can be grown at a wide range of arc current and buffer gas (He) pressure, yet the carbon gas condenses in the fibrous structures only under specific conditions. The deposits are composed of hard shell containing a black core containing CNTs. The growth of the CNTs requires either low arc current at high pressure or high current at low pressure [22].

The photos of cathode deposits formed under lower and higher pressure are shown in Fig. 6. For both pressures roughly 50% of sublimated carbon is deposited on the cathode tip. However, the morphology of both deposits is quite different: at higher pressure the core of the deposit contains much more soft material, which is rich in CNTs.

The morphology of typical carbon structures in the cathode deposit core is shown in Fig. 7. These structures were obtained under pressure 95 kPa and discharge current 60 A.

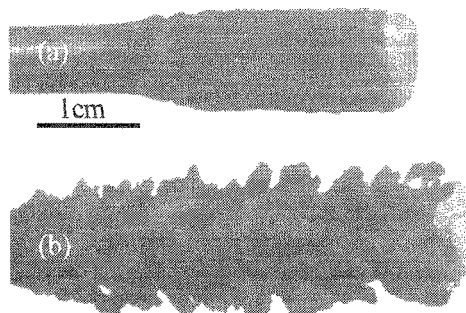


Fig. 6 Photos of cathode deposits formed under pressure (a) - 13 and (b) - 60 kPa.

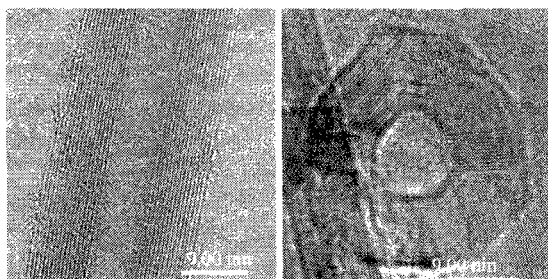


Fig. 7. HRTEM images of CNT (left) and nanocapsule (right) in cathode core. Anode: pure graphite.

Under such conditions multi-walled carbon nanotubes (MWCNTs) grow. Besides of the nanotubes also empty nano-capsules, so called nano-onions, can be found in the deposit.

Co-evaporation of carbon and catalysts in the arc also results in formation of CNTs. However, the CNTs are mostly found in the soot with prevailing single-walled nanostructures (SWCNTs). Moreover, a web-like material is often formed in the reactor [23]. Examples of the HRTEM images of the webs are shown in Fig. 8 when homogeneous graphite electrodes doped with Fe or Co/Ni were used, (a) and (b), respectively.

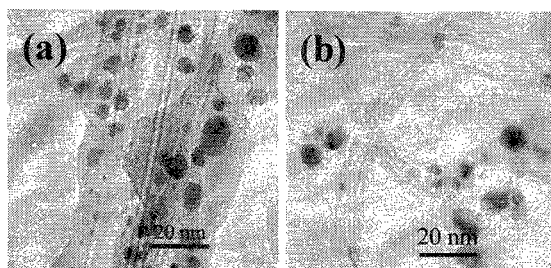


Fig. 8. HRTEM of CNTs in webs. Anode: (a) - C + 0.6 at% Fe; (b) - C + 0.6 at% Co/Ni.

As it is seen in Fig. 8 the most interesting feature of the webs is the presence of CNTs with few only layers. Some catalysts, like e.g., Y mixed with Ni enhance

formation of the single walled carbon nanotubes (SWCNTs). Surprisingly, the yield of the SWCNTs can be significantly more enhanced, even three times, if (in addition to a Ni/Y mixture) the anode contains also fine diamond powder [24]. The same effect we observed when replacing Y by Ce. SEM image of as produced web is shown in Fig. 9. Such a product was obtained under He pressure 80 kPa and discharge current equal to 55 A. One has to admit that diamond lowers significantly electrode conductivity and thereby the anode erosion rate.

The presence of only Gd or Y in graphite electrode drastically changes the dynamics of the anode ablation process and cathode deposit and CNTs formation. Even small admixture of these elements (0.8 at%) favor high erosion rate and growth of unusual long cathode deposit of a very regular structure (Fig. 10).

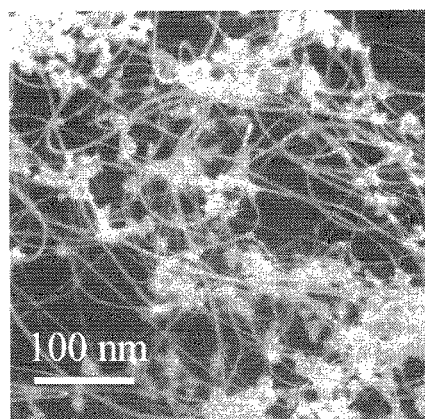


Fig. 9 SEM image of web. Anode: C(sp²) + 10 at% C(sp³) + 1 at% Ni + 0.4 % at Ce .

It is interesting to note that the deposit length does not depend on the anode erosion rate. At lower arc current the deposit is like a hollow cathode with a regular slit along it. At higher current there is only a seam and deposit is filled with a cotton-wool like material with plenty of MWCNTs (Fig. 11).

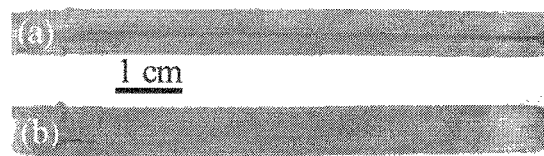


Fig. 10 Photos and SEM of anode deposits formed under pressure 13 kPa.

MWCNTs are formed exclusively in the cathode core (Fig. 12). Some of them are filled with the catalyst (a) and some are of telescopic structure (b). The successful engineering of MWCNTs into fully telescoped structures, which could make ideal-geometry tips for scanned and filed emission microscopy has already been elaborated [25].

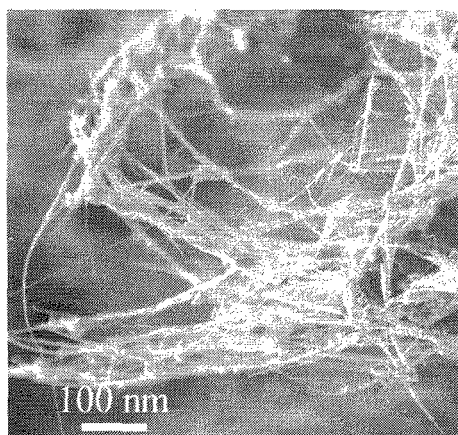


Fig. 11. SEM image of fibrous structures in cathode core. Anode: C + 0.8at% Gd. P: 13.3 kPa.

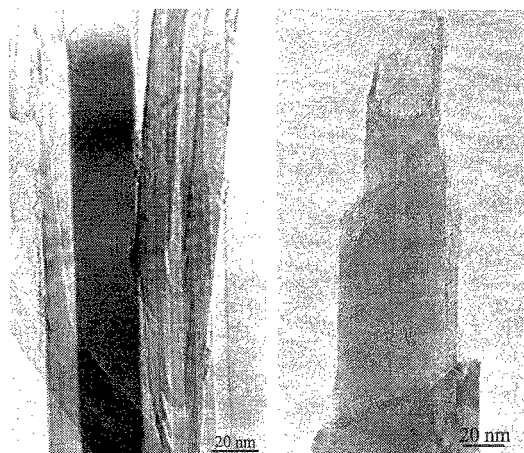


Fig. 12. HRTEM images of CNTs in the cathode core. Anode: C + 0.8at% Gd. P: 60 kPa

We have also found some unexpected and unusual meso- and nanocarbons grown on the surface of the catalyst-containing anodes. The examples are shown in Fig. 13 when Ce-doped anode was used. The process of their formation resembles the CVD growth of carbon fibers on catalyst spots of a substrate.

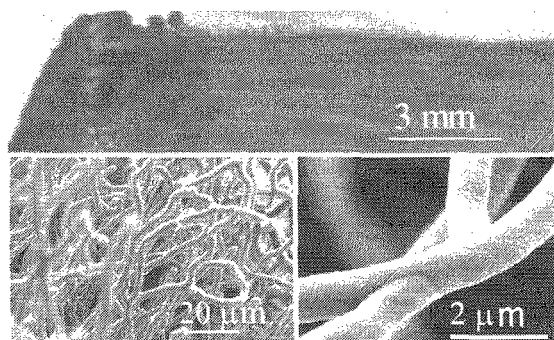


Fig. 13. Anode deposits formed during arc sublimation of Ce-doped anode.

From the practical point of view, an arc discharge in liquid, e.g., in water, is also of high interest [10]. The HRTEM images of carbon nanostructures, depending on the kind of electrodes (pure or doped), are shown in Fig. 14. In the case of discharge between pure graphite electrodes the product, floating on water surface, consisted of carbon nano-onions (a) and MWCNTs (b). High yield and cost-efficient approaches to nano-onions production will probably foster the industrial application, e.g., in lubrication technology. The MWCNTs exhibited no significant differences from those generated by arc discharge in He (Fig. 6). When Gd-doped electrodes were used polygonal encapsulated crystals and isolated NTs filled with the catalyst are apparent, (c) and (d), respectively. Similar structures are formed in the case of Y-doped anode, (e) and (f).

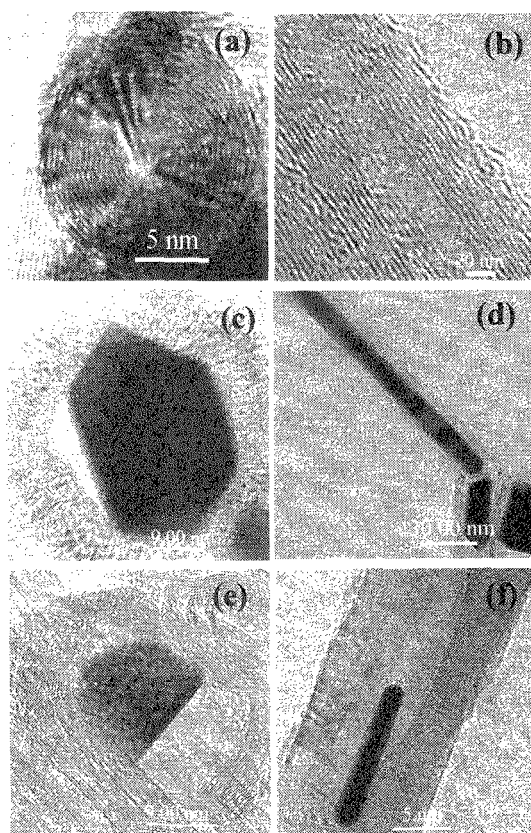


Fig. 14. HRTEM images of nanostructures after arc discharge in water. Products floating on water surface: C- (a and b); C + 0.8 at% Gd - (c and d); C + 0.8 at% Y - (e and f). Cathode deposit: C + 0.8 at% Y - (e).

Our current research is also focused on obtaining nanoencapsulates with magnetic core using the arc plasma. Preliminary experiments were carried out with graphite anode drilled and filled with a magnetic mixture containing Fe, Co, Nd, Pr and B (45, 17, 33, 5 and < 1 wt %, respectively). The arc burned under the pressure 60 kPa and discharge current 80 A. The collected soot did not contain neither fullerenes nor nanotubes, but encapsulates were present. These encapsulates were

separated from other metal particles by solving the latter in a hydrochloric acid. An example of HRTEM image of an encapsulate is shown in Fig. 14. The outer graphene layers and the core, built of magnetic materials, are clearly distinguishable.

Preliminary measurements of magnetic properties revealed that the core could be classified as a hard magnetic material with coercive force 33 kA m^{-1} . Further studies are in progress.

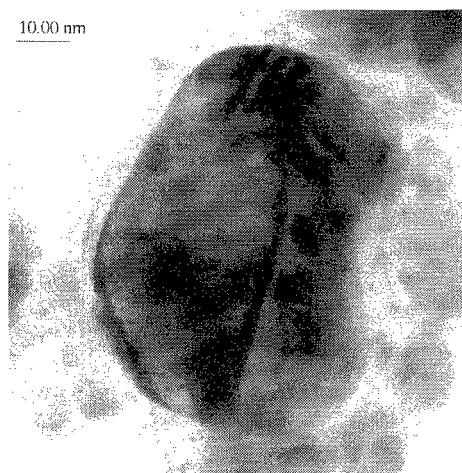


Fig. 14. Carbon encapsulate with crystalline magnetic core. Anode: C + (Fe, Co, Nd, Pr and B).

We have also initiated the research focused at the application of a non-thermal plasma [26] to grow thin films of aligned 1D nanocarbons the formation of which has been reviewed elsewhere [27].

Acknowledgment. The work was supported by the Committee for Scientific Research (KBN) under Grant No. 4 T08D 021 23.

4. REFERENCES

- [1] H. W. Kroto, J.R. Heath, S.C. O'Brien, R.F. Curl and R.E. Smalley, *Nature*, 318, 162-163 (1985).
- [2] W. Krätschmer, L. D. Lamb, K. Fostiropoulos and D. R. Huffman, *Nature*, 347, 354-357 (1996).
- [3] S. Iijima, *Nature*, 354, 56-60 (1991).
- [4] P.M. Ajayan and S. Iijima, *Nature*, 358, 23 (1992).
- [5] T. Brown, *Models Chem.*, 132, 245 (1995).
- [6] W.K. Maser J.M. Lambert, P.M. Ajayan, O. Stephan and P. Bernier, *Synth. Met.*, 77, 243 (1996).
- [7] A.A. Setlur, J.M. Lauerhass, J.Y. Dai and R.P. H. Chang, *Appl. Phys. Lett.*, 69, 345 (1996).
- [8] Y. Saito, K. Nishikubo, K. Kawabata and T. Matsumoto, *J. Appl. Phys.*, 80, 3062 (1996).
- [9] X. Zhao, S. Inoue, M. Jinno, T. Suzuki and Y. Ando, *Chem. Phys. Letters*, 373, 266-271 (2003).
- [10] N. Sano, H. Wang, M. Chhowalla, I.J. Alexandrou and G.A. Amaratunga, *Nature*, 414, 506-507 (2001).
- [11] H.W. Zhu, X.S. Li, B. Jiang, C.L. Xu Y.F. Zhu, D.H. Wu and X.H. Chen, *Chem. Phys. Lett.*, 366, 664-669 (2002).
- [12] H. Lange, M. Sioda, A. Huczko, Y.Q. Zhu, H.W. Kroto and D.R.M. Walton, *Carbon*, 41, 1617-1623 (2003).
- [13] Y.L. Hsin, K.C. Hwang, F.R. Chen and J.J. Kai, *Adv. Mater.*, 13, 830-835 (2001).
- [14] M. Ishigami, J. Cumings, A. Zettl and S. Chen, *Chem. Phys. Lett.*, 319, 457 (2000).
- [15] N.I. Alekseyev and G.A. Dyuzhev, *Carbon*, 41, 1343-1348 (2003).
- [16] H. Lange, P. Baranowski, A. Huczko and P. Byszewski, *Rev. Sci. Instrum.*, 68, 3723-3727 (1997).
- [17] H. Lange, K. Saidane, M. Razafinimanana, A. Gleizes, *J. Phys. D: Appl. Phys.*, 32, 1024-1030 (1999).
- [18] S. Akita, H. Ashihara and Y. Nakayama, *Jpn. J. Appl. Phys.* 39, 8, 4939-4945 (2000).
- [19] H. Lange, A. Huczko, M. Sioda, M. Pacheco, M. Razafinimanana and A. Gleizes, "Progress in Plasma Processing of Materials 2003", Ed. By P. Fauchais, Begell House, N.Y. (2003) pp. 99-104.
- [20] A. Huczko, H. Lange and T. Sogabe, *J. Phys. Chem. A* 104, 10708-10712 (2000).
- [21] H. Lange, A. Huczko, M. Sioda, M. Pacheco, M. Razafinimanana and A. Gleizes, *Plasma Chem. Plasma Process.* 22, 4, 523-535 (2002).
- [22] P. Byszewski and A. Nabałek, *Europhysics Lett.*, 34, 31-33 (1996).
- [23] M. Takizawa, S. Bandow, T. Torii and S. Iijima, *Chem. Phys. Lett.*, 302, 148-154 (1999).
- [24] M. Pacheco, M. Monthieux, M. Razafinimanana, L. Donnadieu, H. Allouche, N. Caprais and A. Gleizes, *Carbon 2000 Int. Conf.*, Beijing (China), no 1014 (CD-Rom).
- [25] A. Zettl and J. Cumings, *Molecular Nanostructures*, ed. H. Kuzmany, J. Fink, M. Mehring and S. Roth, *AIP Conf. Proc.*, 544, 526-532 (2000).
- [26] A. Huczko, H. Lange, M. Sioda, Y.Q. Zhu, W.K. Hsu, H.W. Kroto and D.R.M. Walton, *J. Phys. Chem. B*, 106, 7, 1534-1536 (2002).
- [27] A. Huczko, *Applied Physics A*, 74, 617-638 (2002).

(Received October 8, 2003; Accepted March 12, 2004)